Precambrian Research 295 (2017) 12–23

Contents lists available at ScienceDirect

Precambrian Research

journal homepage: www.elsevier.com/locate/precamres

A predominantly ferruginous condition in the Ediacaran deep ocean: Geochemistry of black shales in the Ediacaran Doushantuo Formation, South China

Jing Huang [a,*], Lianjun Feng [b,c], Xuelei Chu [b,c], Tao Sun [d], Hanjie Wen [e], Liping Qin [a], Yanan Shen [a]

[a] CAS Key Laboratory of Crust-Mantle Materials and Environments, School of Earth and Space Sciences, University of Science and Technology of China, Hefei 230026, China
[b] Institute of Geology and Geophysics, Chinese Academy of Sciences, Beijing 100029, China
[c] Key Laboratory for Mineral Resources, Chinese Academy of Sciences, Beijing 100029, China
[d] Department of Earth and Atmospheric Sciences, University of Houston, Houston, TX 77062, USA
[e] State Key Laboratory of Ore Deposit Geochemistry, Institute of Geochemistry, Chinese Academy of Sciences, Guiyang 550002, China

ARTICLE INFO

Article history:
Received 1 August 2016
Revised 28 February 2017
Accepted 7 April 2017
Available online 13 April 2017

Keywords:
Ediacaran
Deep water
Fe speciation
Trace element
South China

ABSTRACT

The redox condition of the ocean played an important role in the evolution of the Ediacaran biota, but it remains largely unexplored, particularly for the deep ocean environment. In this study, we present a comprehensive study of Fe speciation and trace elements of the Doushantuo black shales from the Longe and Jinjiadong sections in South China, to investigate the redox condition of basinal environments in Ediacaran. In general, both sections show high Fe_{HR}/Fe_T ratios (>0.38), low Fe_{Py}/Fe_{HR} ratios (<0.7), suggesting a predominately anoxic and ferruginous condition in the deep water of Nanhua basin during the Doushantuo period. A few high Fe_{Py}/Fe_{HR} ratios (>0.7) in the Jinjiadong section indicating occasional euxinia in the basin facies. Fe_{Py}/Fe_{HR} ratios show an increase in the middle part both in the Longe and Jinjiadong sections, indicating enhanced production of H_2S via bacteria sulfate reduction (BSR) in the deep anoxic water, which was likely responsible to the upper Doushantuo negative carbon isotope excursion.

The enrichment factors (EFs) of most redox sensitive trace elements in the sediments of both sections are low ($\leq$1), while EF-Mo shows moderately enriched ($\sim$3–60), which is similar to the modern Cariaco Basin. Because of paleogeographic restriction or persistent ocean stratification, the trace elements renewal would be mostly obstructed in the isolated deep water, and their inventory could become depleted, which cause the low EFs of most trace elements in sediments. However, for the non-euxinic deep ocean, a "particulate shuttle" would transport Mo from shallow water to deep water through adsorption-desorption on the Mn–Fe-oxyhydroxides, which maintained moderate Mo enrichment in seawater and related sediments.

1. Introduction

Early animal evolution has been proposed to be intimately associated with the atmosphere and ocean redox chemistry (Knoll, 1992). Lines of evidence support that the emergence and diversification of Ediacaran biota was tied to varying levels of pulsed atmosphere oxygenation during the Ediacaran (Canfield et al., 2007; Fike et al., 2006; McFadden et al., 2008; Och and Shields-Zhou, 2012; Sahoo et al., 2012; Shen et al., 2008). However, the mechanism and extent of this oxygenation event remain largely unconfined, particularly for the redox condition of the Ediacaran deep ocean.

The Ediacaran deep ocean was thought widely oxygenated from perspectives of elemental and isotopic compositions and iron chemistry (Ader et al., 2014; Canfield, 1998; Canfield et al., 2007; Fike et al., 2006). In contrast, more studies suggested that the Ediacaran ocean was stratified with oxic shallow water, while with widespread anoxia in the deep ocean (Canfield et al., 2008; Fan et al., 2014; Han and Fan, 2015; Jiang et al., 2011, 2010, 2008; Li et al., 2010; Och and Shields-Zhou, 2012). In addition, it has been actively debated that whether the anoxic deep ocean was ferruginous or euxinic (Canfield et al., 2008; Li et al., 2010; Shen et al., 2008). Recent oceanic redox model proposed that below the shallow oxic water, a metastable zone of the euxinic water column

* Corresponding author.
E-mail address: hjmail@ustc.edu.cn (J. Huang).

http://dx.doi.org/10.1016/j.precamres.2017.04.019
0301-9268/

may be sandwiched within ferruginous open deep water at the outer shelf and slope locations (Li et al., 2010). These controversies likely were caused by the chemical heterogeneity of the Ediacaran ocean, which was not only introduced by the oxygen level in the atmosphere, but also other factors (e.g. the substance input and paleogeography) (Li et al., 2010; Scott et al., 2008; Tribovillard et al., 2012). Therefore, comprehensive studies with multiple geochemical proxies on more typical sections are important to further decipher the redox state of the Ediacaran ocean.

Here we investigated the redox-sensitive elements and Fe speciation of the black shales that were deposited in basin facies from Doushantuo Formation in South China, which proxy the redox condition of deep water in Nanhua basin during most of the Ediacaran period. In addition, the enrichment mechanism of trace elements also provided new information on the elements migration and paleogeography in Nanhua basin.

2. Geological setting

The Ediacaran System of South China was deposited in a passive continental margin along a paleoseawater depth gradient from the northwest to the southeast on the Yangtze Block (Jiang et al., 2003; Wang and Li, 2003). The Ediacaran System in South China is mostly composed of the Doushantuo Formation (ca. 635–551 Ma) and with Dengying Formation (ca. 551–542 Ma) at the terminal stage. The Ediacaran System directly overlies the Nantuo diamictite (equivalent to the Marinoan glaciation), and was overlain by the lower Cambrian phosphorite-bearing shale (Condon et al., 2005; Jiang et al., 2003; Zhu et al., 2007). The lithology of those strata varies for different sedimentary facies. In the northwest, the carbonate and shale-interbedded (10 m–>100 m) Doushantuo Formation is overlain by the carbonate-predominant (>100 m thick) Dengying Formation, which are deposited in shallow water (i.e., the shelf area); in the southeast, the shale-predominant Doushantuo Formation is overlain by the chert-predominant Liuchapo/Laobao/Piyuancun Formation (equivalent to the Dengying Formation), which was deposited in deep water (i.e., the basin area).

In this study, we investigated two typical sections of the Doushantuo Formation, the Longe and the Jinjiadong sections. The Longe section is located in Longe village of Liping County, southeastern Guizhou Province, comprising the Nantuo Formation, the Doushantuo Formation, and the Laobao Formation (Fig. 1). The Doushantuo Formation in the Longe section is approximately 35 m thick and is characterized by the basal cap carbonate (~2.5 m) and the upper black shale (Fig. 1), which were deposited in basin facies. The Jinjiadong section is located in Jinjiadong village of Xupu County, Hunan Province, comprising the Nantuo Formation, the Doushantuo Formation, and the Liuchapo Formation (Fig. 1). The Doushantuo Formation in the Jinjiadong section is approximately 25 m thick and is characterized by the basal cap carbonate (~1.5 m) and the upper black shale (Fig. 1), which were deposited in basin facies.

3. Sample and method

Large hand samples of black shales were collected by digging in depth from the outcrop site. The surface of hand samples were removed, and the inner parts were chosen carefully to avoid possible weathering impact on the geochemical analyses. To avoid the contamination from analytical procedures, the samples were ground (<200 mesh) with agate mortar and pestle for elemental and isotopic analyses. 28 samples from the Longe section and 21 samples from the Jinjiadong section were selected for the geochemical analysis.

About 50 mg of each sample powder from the Longe section was weighed and ashed at 450 °C for 12 h. Dissolution of the ashed samples was carried out using HNO_3 and HF (Qi et al., 2000). For each ashed sample, 1 ml of HF (38%) and 0.5 ml of HNO_3 (68%) were added in a Teflon bomb, and the solution was heated to dryness. Then 1 ml of HF and 0.5 ml of HNO_3 were added again to dissolve the solid materials completely, and the sealed bomb was heated to 190 °C for 12 h. After cooling, 1 ml of Rh solution (1 mg/ml) was added as an internal standard, and the solution was again heated to dryness (at about 150 °C). Addition of 1 ml of HNO_3 and subsequent heating to dryness was repeated twice. The final residue was dissolved in 8 ml of 40% HNO_3, and the sealed bomb was heated at 110 °C for a period of 3 h. The solutions were subsequently analyzed by Induced Coupled Plasma-Mass Spectrometer (ICP-MS) at the Key Laboratory of Ore Deposit Geochemistry, Institute of Geochemistry, Chinese Academy of Sciences, Guiyang. Based on duplicate analysis, the analytical precision is better than 8% for all of the analyzed trace metals. Similar proce-

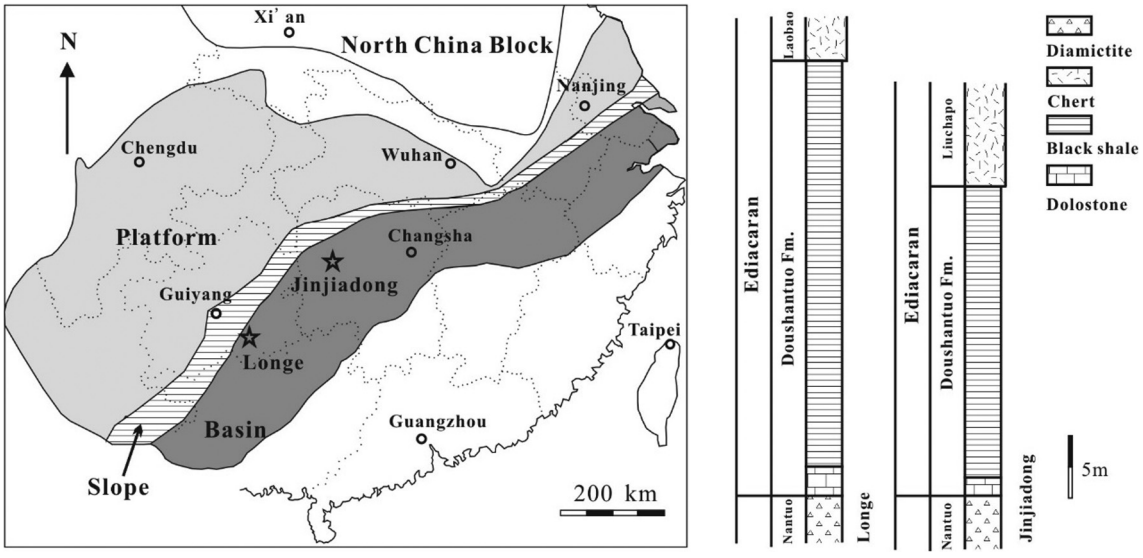

Fig. 1. Paleogeographic reconstruction of the Ediacaran Doushantuo Formation (modified after Jiang et al., 2011), the study regions in South China, and the stratigraphic column.

Table 1
Fe speciations, TOC, trace elements and $\delta^{34}S_{py}$ variations from the Doushantuo black shales in the Longe section.

Sample	Depth (m)	Al_2O_3 (%)	S (%)	TOC (%)	V (ppm)	Cr (ppm)	Co (ppm)	Cu (ppm)	Zn (ppm)	Ni (ppm)	Mo (ppm)	U (ppm)	Fe_{carb} (%)	Fe_{oxide} (%)	Fe_{mag} (%)	Fe_{py} (%)	Fe_{HR} (%)	Fe_T (%)	Fe_{py}/Fe_{HR}	Fe_{HR}/Fe_T	$\delta^{34}S_{py}$ (‰)
LE07-01	2.6	13.07	0.09	1.31	97.00	50.00	0.60	11.00	16.00	6.00	6.00	2.33	0.03	0.39	0.16	0.02	0.60	1.06	0.04	0.56	
LE07-02	2.9	15.72	0.05	1.03	149.00	60.00	0.60	8.00	21.00	7.00	7.00	3.88	0.03	0.20	0.16	0.03	0.43	0.84	0.07	0.51	
LE07-04	3.5	15.02	0.08	3.24	242.00	70.00	0.80	10.00	20.00	2.50	21.00	3.97	0.04	0.32	0.19	0.01	0.55	0.95	0.01	0.58	
LE07-06	4.1	14.99	0.05	0.81	235.00	80.00	1.90	12.00	20.00	9.00	9.00	5.08	0.06	0.09	0.03	0.01	0.19	0.41	0.05	0.48	
LE07-08	4.7	15.82	0.20	1.65	251.00	100.00	0.90	19.00	16.00	5.00	8.00	5.95	0.04	0.43	0.30	0.00	0.77	1.14	0.00	0.67	
LE07-10	5.3	15.27	0.07	2.76	269.00	110.00	0.90	6.00	17.00	7.00	4.00	4.25	0.09	0.09	0.02	0.00	0.20	0.37	0.01	0.55	
LE07-12	5.9	14.99	0.06	1.83	370.00	120.00	0.50	15.00	17.00	7.00	9.00	4.59	0.05	0.35	0.30	0.01	0.71	1.10	0.02	0.65	
LE07-14	6.5	16.77	0.13	0.73	336.00	90.00	0.50	11.00	14.00	2.50	3.00	4.60	0.06	0.25	0.17	0.02	0.50	0.78	0.03	0.64	15.35
LE07-16	7.1	16.45	0.04	0.27	244.00	60.00	0.25	6.00	19.00	2.50	2.00	3.11	0.04	0.24	0.13	0.00	0.41	0.73	0.00	0.56	
LE07-18	7.7	15.10	0.03	2.26	244.00	70.00	0.50	12.00	21.00	2.50	4.00	3.71	0.04	0.16	0.11	0.00	0.31	0.58	0.00	0.54	
LE07-21	8.6	15.66	0.03	1.19	227.00	70.00	1.80	17.00	20.00	8.00	3.00	3.86	0.11	0.20	0.13	0.00	0.45	0.69	0.01	0.65	
LE07-24	9.5	16.51	0.01	0.47	164.00	70.00	7.90	26.00	42.00	12.00	1.00	2.46	0.09	0.32	0.28	0.00	0.69	1.04	0.00	0.67	
LE07-27	10.7	7.51	0.06	1.69	111.00	30.00	1.80	18.00	12.00	15.00	1.00	1.92	0.28	0.39	0.25	0.01	0.93	1.41	0.01	0.66	
LE07-30	11.6	7.41	0.05	1.22	91.00	30.00	7.30	18.00	138.00	37.00	1.00	1.39	0.07	0.46	0.37	0.00	0.90	2.42	0.00	0.37	
LE07-33	12.5	6.86	0.03	1.12	95.40	31.03	1.20	21.50	31.20	4.89	1.41	1.51	0.35	0.55	0.61	0.02	1.53	2.29	0.01	0.67	
LE07-35	13.1	8.99	0.03	1.60	163.00	63.92	0.77	15.90	18.80	14.16	2.21	2.87	0.14	0.21	0.18	0.01	0.54	0.74	0.01	0.73	
LE07-36	15.4	12.60	0.02	0.46	240.00	77.12	0.85	12.30	20.40	16.21	1.85	3.84	0.14	0.19	0.13	0.01	0.47	0.70	0.02	0.67	
LE07-38	16.2	5.51	0.08	1.54	38.50	31.38	3.33	43.10	46.60	11.49	0.86	2.47	0.11	0.47	0.29	0.01	0.87	1.72	0.01	0.51	
LE07-39	17	13.62	0.04	4.11	147.00	86.70	0.36	17.10	24.10	5.61	6.63	11.70	0.02	0.14	0.07	0.00	0.23	0.31	0.02	0.75	
LE07-40	18	12.86	0.39	5.86	200.00	85.10	0.75	17.50	23.50	8.90	20.40	8.82	0.03	0.24	0.11	0.12	0.49	0.54	0.23	0.91	12.60
LE07-41	19	10.56	1.13	6.22	134.00	71.01	2.00	12.50	20.50	14.96	16.70	7.77	0.06	0.23	0.13	0.50	0.92	1.21	0.54	0.76	13.64
LE07-42	20	11.28	0.36	8.00	136.00	87.23	0.77	20.70	77.70	12.91	15.70	8.97	0.15	0.47	0.24	0.10	0.96	1.49	0.10	0.64	
LE07-43	21	13.01	0.07	6.49	205.00	115.24	2.11	23.50	235.00	28.23	24.00	19.80	0.09	0.70	0.42	0.01	1.21	1.79	0.01	0.68	
LE07-44	29	12.16	0.24	6.11	198.00	109.04	0.77	28.10	36.60	11.13	21.20	11.30	0.02	0.49	0.24	0.01	0.75	1.22	0.01	0.62	
LE07-45	30	8.21	0.12	8.26	125.00	92.19	9.00	85.30	216.00	62.24	15.30	19.00	0.10	0.89	0.66	0.04	1.69	3.05	0.02	0.55	
LE07-46	32	10.48	0.17	14.30	153.00	180.84	0.82	63.90	46.10	21.91	18.50	13.40	0.09	0.52	0.35	0.01	0.97	1.32	0.01	0.73	8.49
LE07-47	33	11.92	0.17	6.36	113.00	147.16	0.89	64.40	72.00	20.66	10.60	9.15	0.08	0.55	0.18	0.02	0.83	1.31	0.03	0.63	25.29
LE07-48	34	10.84	0.61	12.01	138.00	141.84	0.85	98.40	33.80	91.72	15.30	10.70	0.06	0.41	0.18	0.35	1.01	1.34	0.35	0.76	22.27

dure of digestion was carried for the samples from the Jinjiadong section, and the solutions were subsequently analyzed by a PerkinElmer DRCII ICP-MS at University of Science and Technology of China (USTC). Based on duplicate analysis, the analytical precision is better than 8% for all of the analyzed trace metals.

Total Fe (Fe_T) and Al contents were determined on a Shimadzu X-ray fluorescence spectrometer (XRF-1500) at the State Key Laboratory of Lithospheric Evolution, Institute of Geology and Geophysics, Chinese Academy of Sciences, Beijing, and the analytical precision is better than 5%. Total organic carbon (TOC) contents were measured by a Flash HT Elemental analyzer at the Biogeochemistry Laboratory of USTC, and the analytical precision is better than 5%. The enrichment factors (EFs), as used in previous studies, are applied to describe the authigenic trace elements enrichment with the equation $EF\text{-}X = [(X/Al)_{sample}/(X/Al)_{PAAS}]$ (Tribovillard et al., 2006). The values of X and Al refer to their weight concentrations, and the PAAS (post-Archean average shale) data for normalization were from Taylor and McLennan (1985).

The highly reactive iron (Fe_{HR}) consists of iron in pyrite (Fe_{py}), carbonate-associated iron (Fe_{carb}), ferric oxides (Fe_{ox}) and magnetite (Fe_{mag}). Following a previously described procedure (Li et al., 2010), the extractions for Fe_{carb}, Fe_{ox} and Fe_{mag} were carried out at the Biogeochemistry Lab of USTC. The extracts were analyzed for the Fe contents using an Atomscan Advantage ICP-AES at the Public Experimentation Center of USTC, and the analytical precision is better than 5%. Pyrite extraction and quantification was carried out by using the chromium reduction method with silver nitrate traps (Arnold et al., 2014), and Fe_{py} was calculated stoichiometrically based on the concentration of sulfur in pyrite. The sulfur isotopic composition of pyrite ($\delta^{34}S_{py}$) was measured by online combustion of Ag_2S precipitates with an excess of V_2O_5 on a Thermo Delta V Plus isotope ratios mass spectrometer coupled with a Costech elemental analyzer at the State Key Laboratory of Lithospheric Evolution, Institute of Geology and Geophysics, Chinese Academy of Sciences, Beijing. Sulfur isotopes are reported in standard δ-notation relative to Vienna Canon Diablo Troilite (VCDT). Analytical precision for $\delta^{34}S_{py}$ of the sample set from replicate analyses of IAEA standards (IAEA S1, S2 and S3) is better than ±0.3‰ (1σ; SD).

The samples were cracked, and the fresh surfaces were polished. After coating with gold, the electron microscopic analysis was carried out immediately (Xu et al., 2015). The observations were under the secondary electron mode (SE) and backscatter electronic (BSE) mode respectively on an FEI Sirion 200 Scanning electron microscope (SEM) at CAS Key Laboratory of Crust-Mantle Materials and Environments in USTC. The SEM electron beam was set at 15 kV and 18 nA. An energy dispersive spectrometry (EDS) Oxford Inca XMax 50 equipped with the SEM were used to identify and quantify major element for the minerals.

4. Results

4.1. Longe section

Fe speciation, trace element concentration, TOC, and $\delta^{34}S_{py}$ of the samples from the Longe section are listed in Table 1 and are plotted in Fig. 2. Fe_T values range between 0.31% and 3.05%, and Fe_{HR} values range between 0.19% and 1.69%. Most Fe_{HR}/Fe_T values exceed 0.38, except one sample (0.37). Most Fe_{py}/Fe_{HR} values are very low (<0.1) due mainly to very low Fe_{py} (<0.05%). Some samples in the middle part (around 14.5 m) show relatively high Fe_{py} contents (>0.1%), and their Fe_{py}/Fe_{HR} values are relatively high (up to 0.54). However, all the Fe_{py}/Fe_{HR} ratios are lower than 0.7. The TOC are relatively high (>5%) in the upper part (above 14.5 m) while low in the lower part (<5%).

For most trace elements (V, Cr, Co, Ni, Cu, and Zn), the concentrations are equal to or less than the average shale values (Table 1). Thus, the enrichment factors of these elements are equal to or less than 1 (Table 2; Fig. 3). Mo concentrations range between 0.86 ppm to 24.00 ppm, and the EF-Mo range between 1.14 and 35.22. U concentrations range between 1.39 ppm and 19.80 ppm, and the EF-U range between 0.91 and 14.11. The EF-Mo and EF-U show similar variation trends with TOC.

4.2. Jinjiadong section

Fe speciation, trace element concentration, TOC, and $\delta^{34}S_{py}$ of the samples from the Jinjiadong section are listed in Table 3 and

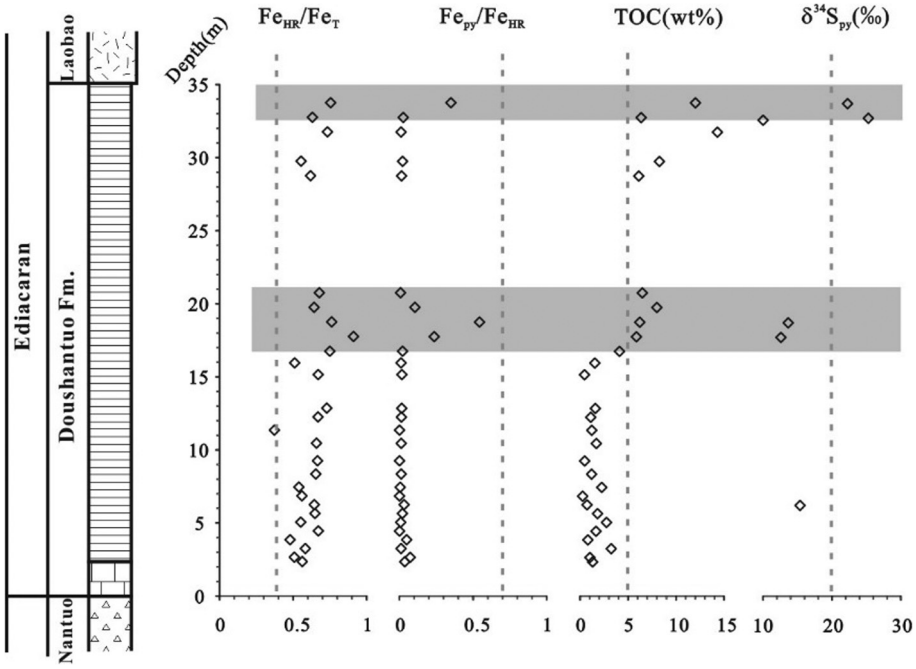

Fig. 2. Fe speciation, TOC, and $\delta^{34}S_{py}$ variations from the Doushantuo black shales in the Longe section.

Table 2
Enrichment factors of trace elements from the Doushantuo black shales in the Longe section.

Sample	Depth (m)	EF-V	EF-Cr	EF-Co	EF-Cu	EF-Zn	EF-Ni	EF-Mo	EF-U
LE07-01	2.6	0.94	0.66	0.04	0.32	0.27	0.16	8.68	1.09
LE07-02	2.9	1.19	0.66	0.03	0.19	0.30	0.15	8.42	1.50
LE07-04	3.5	2.03	0.80	0.04	0.25	0.30	0.06	26.42	1.61
LE07-06	4.1	1.98	0.92	0.10	0.30	0.30	0.21	11.35	2.07
LE07-08	4.7	2.00	1.09	0.05	0.45	0.22	0.11	9.56	2.29
LE07-10	5.3	2.22	1.24	0.05	0.15	0.25	0.16	4.95	1.70
LE07-12	5.9	3.11	1.38	0.03	0.38	0.25	0.16	11.35	1.87
LE07-14	6.5	2.52	0.92	0.02	0.25	0.19	0.05	3.38	1.67
LE07-16	7.1	1.87	0.63	0.01	0.14	0.26	0.05	2.30	1.15
LE07-18	7.7	2.04	0.80	0.03	0.30	0.31	0.06	5.01	1.50
LE07-21	8.6	1.83	0.77	0.09	0.41	0.28	0.18	3.62	1.50
LE07-24	9.5	1.25	0.73	0.39	0.60	0.57	0.25	1.14	0.91
LE07-27	10.7	1.86	0.69	0.20	0.91	0.36	0.69	2.52	1.56
LE07-30	11.6	1.55	0.70	0.81	0.92	4.14	1.72	2.55	1.14
LE07-33	12.5	1.75	0.78	0.14	1.18	1.01	0.24	3.88	1.34
LE07-35	13.1	2.28	1.22	0.07	0.67	0.46	0.54	4.65	1.95
LE07-36	15.4	2.40	1.05	0.06	0.37	0.36	0.44	2.78	1.86
LE07-38	16.2	0.88	0.98	0.50	2.96	1.88	0.72	2.95	2.73
LE07-39	17	1.36	1.09	0.02	0.47	0.39	0.14	9.20	5.24
LE07-40	18	1.96	1.14	0.05	0.51	0.41	0.24	29.98	4.18
LE07-41	19	1.60	1.16	0.16	0.45	0.43	0.49	29.89	4.49
LE07-42	20	1.52	1.33	0.06	0.69	1.53	0.39	26.31	4.85
LE07-43	21	1.99	1.52	0.13	0.68	4.02	0.75	34.87	9.28
LE07-44	29	2.05	1.54	0.05	0.87	0.67	0.31	32.95	5.67
LE07-45	30	1.92	1.93	0.90	3.93	5.85	2.61	35.22	14.11
LE07-46	32	1.84	2.96	0.06	2.30	0.98	0.72	33.36	7.80
LE07-47	33	1.19	2.12	0.06	2.04	1.34	0.60	16.81	4.68
LE07-48	34	1.60	2.25	0.06	3.43	0.69	2.91	26.68	6.02

are plotted in Fig. 4. Fe_T values range between 0.16% and 5.50%, and Fe_{HR} values range between 0.05% and 5.06%. Most Fe_{HR}/Fe_T values exceed 0.38, except three samples (<0.38, but >0.15). Most samples show very low Fe_{py} (<0.06%), so most Fe_{py}/Fe_{HR} values are very low (<0.1). Some samples in the basal, middle and top part show relatively high Fe_{py} contents (>0.2%), and their Fe_{py}/Fe_{HR} values are relatively high (up to 0.93). The samples in the top part show high TOC values (>4.5%), and those in lower part are relatively low (<4.5%).

For most trace elements (Cr, Co, Ni, Cu, Zn, and U), the concentrations are equal to or less than the average shale values (Table 3). Thus, the enrichment factors of these elements are equal to or less than 1 (Table 4; Fig. 5). Mo concentrations range between 0.07 ppm and 26.99 ppm, and the EF-Mo range between 0.10 and 54.69. V concentrations range between 14.49 ppm and 414.48 ppm, and the EF-V range between 0.89 and 11.90.

5. Discussion

5.1. The iron speciation and sulfur isotope

The Fe speciation has been one of most important proxies to distinguish the paleoredox conditions in the ocean, by assessing the limitation of reactive iron in the sediments (Poulton and Canfield, 2011). Extensive investigations of modern and ancient sediments showed that the Fe_{HR}/Fe_T ratios in most sediments deposited beneath anoxic bottom waters were higher than 0.38 (Poulton and Raiswell, 2002; Raiswell and Canfield, 1998; Raiswell et al., 2001). Some research further indicated that thermal alteration would cause a loss of Fe_{HR}, and this threshold value should be reduced to 0.15 for some ancient sedimentary rocks, including the Doushantuo Formation sediments (Li et al., 2010; Raiswell et al., 2008). Furthermore, the ferric oxides, magnetite,

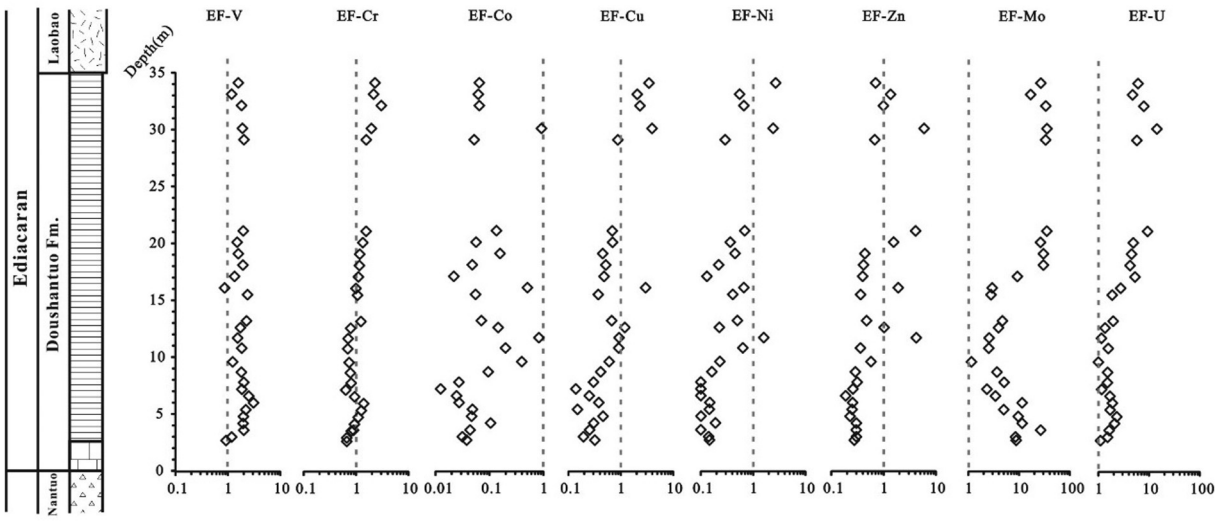

Fig. 3. Enrichment factors of trace element from the Doushantuo black shales in the Longe section.

Table 3
Fe speciations, TOC, trace elements and $\delta^{34}S_{py}$ variations from the Doushantuo black shales in the Jinjiadong section.

Sample	Depth (m)	Al (%)	S (%)	TOC (%)	V (ppm)	Cr (ppm)	Co (ppm)	Cu (ppm)	Zn (ppm)	Ni (ppm)	Mo (ppm)	U (ppm)	Fe_{carb} (%)	Fe_{oxide} (%)	Fe_{mag} (%)	Fe_{py} (%)	Fe_{HR} (%)	Fe_T (%)	Fe_{py}/Fe_{HR}	Fe_{HR}/Fe_T	$\delta^{34}S_{py}$ (‰)
JD17	3.60	7.46	4.57	0.36	261.81	62.87	42.51	55.36	68.50	36.97	23.18	2.04	0.00	0.28	0.01	4.00	4.30	4.63	0.93	0.93	
JJD01	4.70	7.56	0.29	1.55	173.28	44.04	9.59	7.66	4.79	0.47	2.08	0.44	0.02	0.04	0.01	0.25	0.31	0.30	0.80	1.04	11.00
JJD02	5.40	6.26	0.00	1.29	240.39	42.98	9.49	3.98	3.98	0.73	4.86	0.31	0.01	0.01	0.02	0.00	0.05	0.30	0.00	0.15	
JJD03	6.00	5.86	0.00	2.30	240.35	40.85	10.46	3.80	5.70	2.95	12.33	0.07	0.02	0.06	0.01	0.00	0.09	0.28	0.00	0.32	
JJD04	6.90	6.96	0.07	3.45	225.51	46.04	9.07	4.70	4.70	0.91	10.47	0.53	0.00	0.18	0.05	0.06	0.29	0.55	0.21	0.52	
JJD05	7.90	6.70	0.00	1.60	154.19	35.43	12.56	2.87	3.83	0.65	2.99	0.41	0.00	0.14	0.05	0.00	0.19	0.48	0.00	0.40	
JJD06	10.40	3.79	0.00	2.78	143.78	46.99	0.29	1.88	2.82	1.44	4.43	0.50	0.01	0.25	0.06	0.00	0.32	0.55	0.00	0.58	
JJD07	11.60	4.35	0.00	1.55	93.76	51.67	0.21	2.87	3.83	0.91	2.53	0.57	0.01	0.05	0.03	0.00	0.09	0.16	0.00	0.53	
JJD09	14.10	1.80	0.00	1.01	208.96	20.51	57.02	34.18	6.84	5.75	1.93	0.59	0.05	0.08	0.02	0.00	0.14	0.32	0.00	0.45	
JJD10	15.10	2.56	0.00	1.37	294.72	28.21	71.10	40.85	3.89	1.01	3.90	1.52	0.05	0.06	0.03	0.00	0.14	0.30	0.00	0.46	
JJD11	16.10	2.32	0.00	2.98	414.48	34.30	37.06	4.76	2.86	1.26	12.70	1.51	0.04	0.06	0.03	0.00	0.14	0.26	0.00	0.55	
JJD12	16.40	3.27	0.00	2.37	78.63	53.05	0.40	1.89	2.84	2.79	2.00	0.27	0.01	0.09	0.02	0.00	0.11	0.24	0.00	0.48	
JJD13	16.60	5.88	3.77	2.07	122.53	51.87	8.79	32.20	6.26	9.75	1.99	0.23	0.02	0.51	0.13	3.30	3.95	4.06	0.84	0.97	13.50
JJD14	17.60	0.70	0.00	0.63	14.49	15.46	1.37	5.80	23.18	3.83	1.04	0.22	0.00	0.19	0.01	0.00	0.20	0.43	0.00	0.48	
JJD15	17.70	8.51	0.07	2.40	114.06	43.94	6.42	4.67	4.67	2.07	0.85	0.54	0.00	0.03	0.02	0.06	0.11	0.29	0.55	0.38	
JJD16	18.70	6.62	0.05	1.95	94.95	43.24	0.86	3.76	6.58	3.25	0.07	0.23	0.00	0.06	0.02	0.04	0.12	0.30	0.33	0.40	
JJD18	21.70	5.04	0.77	2.58	78.53	53.59	0.94	3.70	4.62	4.22	4.79	0.12	0.00	0.22	0.06	0.67	0.95	2.33	0.71	0.41	8.90
JJD19	22.30	7.20	0.25	2.53	159.89	42.76	13.75	2.79	2.79	6.03	13.02	1.14	0.01	0.08	0.02	0.22	0.32	0.46	0.68	0.69	9.50
JJD20	22.80	5.87	4.58	9.08	188.91	117.20	64.00	78.65	52.43	158.06	26.99	3.65	0.28	0.67	0.10	4.01	5.06	5.15	0.79	0.98	9.00
JJD21	23.40	4.52	3.41	5.48	235.30	92.79	22.29	125.11	176.47	123.86	11.81	2.56	0.02	0.81	0.15	2.98	3.95	5.50	0.75	0.72	14.40
JJD22	24.20	2.30	2.22	4.76	71.75	54.03	25.86	73.52	81.49	61.65	4.56	1.98	0.05	0.44	0.07	1.94	2.51	3.02	0.77	0.83	9.10

and Fe-associated carbonate occur at elevated concentrations in marine sediments as a result of deposition beneath an Fe(II)-containing water column, and they were also constrained by dissolved sulfide due to their proactive reactions (Canfield and Berner, 1987; Poulton and Canfield, 2005). Thus, Fe_{Py}/Fe_{HR} ratio can reflect whether dissolved sulfide or Fe(II) is predominant in the water column. The previous investigations also showed that, if the water column was euxinic, Fe_{Py}/Fe_{HR} ratios in the underlying sediments usually exceeded 0.7 (Anderson and Raiswell, 2004; März et al., 2008; Raiswell and Canfield, 1998).

Most samples in the Longe and Jinjiadong sections show that the Fe_{HR}/Fe_T ratios exceed 0.38, with a few exceptions from the Jinjiadong section but still exceeding 0.15 (Tables 1 and 3; Figs. 2, 4 and 6). These high Fe_{HR}/Fe_T ratios support an anoxic condition in the deep water of Nanhua basin during the Doushantuo period. All the Fe_{Py}/Fe_{HR} ratios in the Longe section are much lower than 0.7 (Figs. 2 and 6), indicating a predominately ferruginous condition. Most Fe_{Py}/Fe_{HR} ratios in the Jinjiadong section are much lower than 0.7, but some samples in the basal, middle and top parts show high Fe_{Py}/Fe_{HR} ratios close to or exceeding 0.7 (Figs. 4 and 6), indicating that the depositional environment was predominantly ferruginous, with occasional euxinic conditions during the initial, middle and terminal Doushantuo period.

The shales in the Longe section mainly consist clay minerals and quartz (Fig. 7A and B). Rich carbon also can be detected accompanied with the clay minerals, which would be the organic carbon that is adsorbed on the clay minerals. There is no framboid pyrite identified by the mineral shapes and structures in the Longe shales (Wignall and Newton, 1998; Wilkin et al., 1996, 1997) (Fig. 7). Some small and amorphous iron oxides scatter in the samples, and very few pyrites with good crystal shape can be observed in the samples (Fig. 7A and B). The sparse distribution of pyrites show that the H_2S was limited in the depositional condition. The siderites are common accompanying with the carbonate minerals (Fig. 7C and D), also suggesting that no available H_2S incorporated with the Fe^{2+} during the deposition process. A few minerals containing sulfur were identified as the barite (Fig. 7E and F), implying that the limited sulfur preferred occurring as sulfate rather than sulfide. These results further indicate that the iron mainly presents as iron oxides, siderites, or possible iron-bearing silicates in the Longe shales, suggesting a non-euxinic condition. It is consistent to the Fe speciation results.

This study suggests a ferruginous condition in the deep ocean of the Nanhua basin during the Doushantuo period. Chang et al. (2010, 2012) studied the sediments of the Laobao Formation (equivalent to the Dengying Formation), and supports that deep water in the Nanhua Basin was also anoxic and ferruginous during the terminal Ediacaran. Han and Fan (2015) reported averagely higher Fe_{Py}/Fe_{HR} ratios (~0.5–0.9) in the Ediacaran sediments from the basinal Xiangtan section in South China, but most of them are still lower than 0.7, also indicating a predominantly ferruginous condition. In the Wuhe section that was located paleogeographically on the middle-lower slope of the Nanhua basin, most sediments have Fe_{Py}/Fe_{HR} ratios exceeding 0.7, indicating persistent euxinia (Sahoo et al., 2016). These results seem to support the "sulfidic water wedge" model of the Ediacaran ocean that was proposed by Li et al. (2010) (Fig. 8).

It is noted that Fe_{Py}/Fe_{HR} ratios show an obvious increase in the middle part in both Longe and Jinjiadong section despite that majority are much lower than 0.7 (Figs. 2 and 4). The increase of Fe_{Py}/Fe_{HR} ratios indicates that the production of H_2S via bacteria sulfate reduction (BSR) was enhanced. The rough covariation between Fe_{Py}/Fe_{HR} ratios and TOC in the Longe section is consistent with increased production/input of organic matter that would enhance BSR and H_2S production (Fig. 2). However, most samples in the Longe and Jinjiadong sections have very little or no pyrite

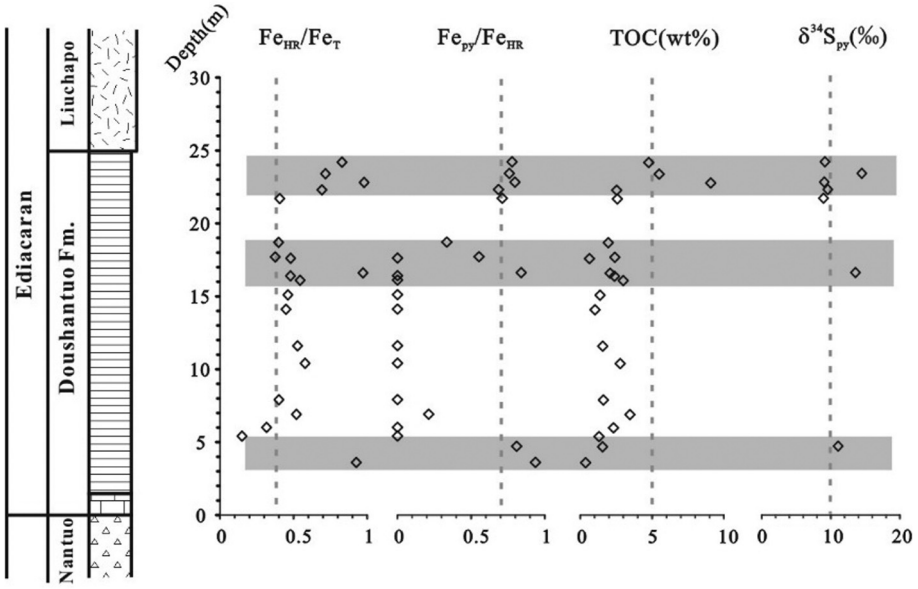

Fig. 4. Fe speciation, TOC, and $\delta^{34}S_{py}$ variations from the Doushantuo black shales in the Jinjiadong section.

Table 4
Enrichment factors of trace elements from the Doushantuo black shales in the Jinjiadong section.

Sample	Depth (m)	EF-V	EF-Cr	EF-Co	EF-Cu	EF-Zn	EF-Ni	EF-Mo	EF-U
JD17	3.60	2.34	0.77	2.48	1.49	1.08	0.90	31.10	0.88
JJD01	4.70	1.53	0.53	0.55	0.20	0.07	0.01	2.75	0.19
JJD02	5.40	2.56	0.63	0.66	0.13	0.07	0.02	7.78	0.16
JJD03	6.00	2.74	0.63	0.78	0.13	0.11	0.09	21.06	0.04
JJD04	6.90	2.16	0.60	0.57	0.14	0.08	0.02	15.05	0.25
JJD05	7.90	1.53	0.48	0.82	0.09	0.07	0.02	4.46	0.20
JJD06	10.40	2.53	1.13	0.03	0.10	0.09	0.07	11.70	0.42
JJD07	11.60	1.44	1.08	0.02	0.13	0.10	0.04	5.81	0.42
JJD09	14.10	7.76	1.04	13.81	3.81	0.45	0.58	10.77	1.05
JJD10	15.10	7.69	1.00	12.10	3.20	0.18	0.07	15.26	1.92
JJD11	16.10	11.90	1.34	6.94	0.41	0.14	0.10	54.69	2.09
JJD12	16.40	1.61	1.48	0.05	0.12	0.10	0.16	6.12	0.26
JJD13	16.60	1.39	0.80	0.65	1.10	0.13	0.30	3.38	0.13
JJD14	17.60	1.39	2.02	0.86	1.67	3.93	1.00	15.02	1.01
JJD15	17.70	0.89	0.47	0.33	0.11	0.06	0.04	1.00	0.21
JJD16	18.70	0.96	0.59	0.06	0.11	0.12	0.09	0.10	0.11
JJD18	21.70	1.04	0.97	0.08	0.15	0.11	0.15	9.52	0.08
JJD19	22.30	1.48	0.54	0.83	0.08	0.05	0.15	18.12	0.51
JJD20	22.80	2.15	1.82	4.75	2.68	1.05	4.90	46.04	2.01
JJD21	23.40	3.47	1.87	2.14	5.54	4.59	4.98	26.14	1.83
JJD22	24.20	2.08	2.14	4.89	6.39	4.17	4.87	19.83	2.78

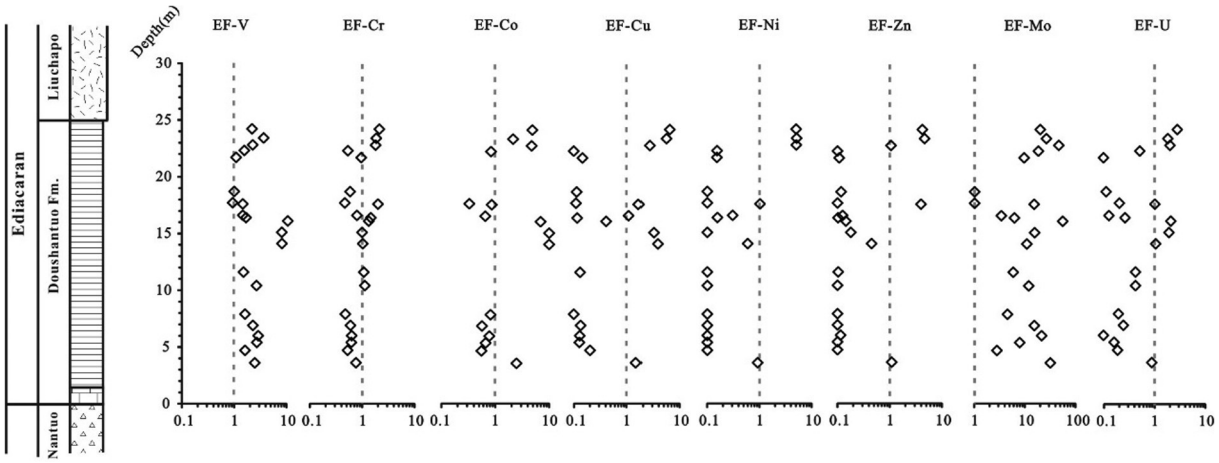

Fig. 5. Enrichment factors of trace element from the Doushantuo black shales in the Jinjiadong section.

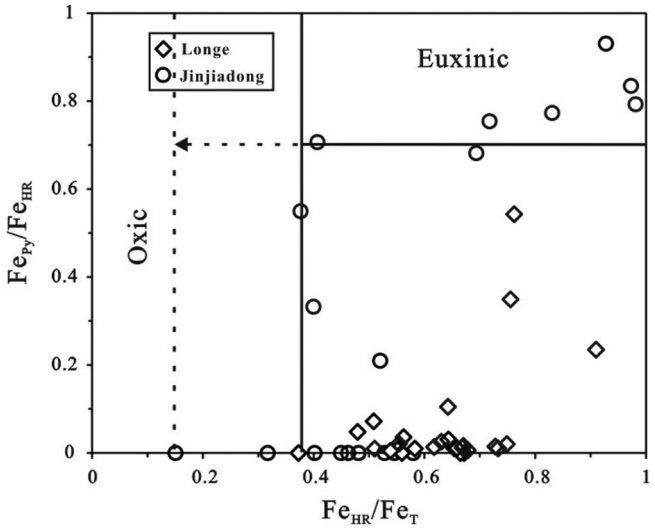

Fig. 6. Fe_{Py}/Fe_{HR} versus Fe_{HR}/Fe_T data for samples from the Doushantuo black shales in the Longe and Jinjiadong section.

(Fe_{Py}/Fe_{HR} < 1%), yet high organic C contents (TOC > 1%) was found in them (Tables 1 and 3). The low pyrite S/TOC ratios suggest that it was sulfate availability rather than organic matter supply limiting the BSR in the deep water of the Nanhua Basin (Fig. 9) (Berner and Raiswell, 1984; Li et al., 2010). Furthermore, with appropriate estimation of the sulfur isotopic compositions (~+20‰) in deep water based on the carbonate-associated sulfate (CAS) from Doushantuo cap carbonates in the Longe section (Huang et al., 2013), the positive $\delta^{34}S_{Py}$ values in this study (mostly >10‰) suggest low fractionations ($\Delta^{34}S$<10‰) associated with BSR, which is consistent with low SO_4^{2-} concentrations in deep water (Habicht and Canfield, 2001; Habicht et al., 2002; Li et al., 2010; Ries et al., 2009). These observations are in line with the previous studies that a large and long-stable organic matter pool with very small sulfate concentrations existed in the Ediacaran deep water of Nanhua basin (Jiang et al., 2007, 2010, 2008; McFadden et al., 2008; Rothman et al., 2003). Therefore, increased sulfate input to deep water possibly have played a more important role to enhance BSR and H_2S production.

More work is needed to determine the primary mechanism of the enhanced BSR and H_2S production during the middle Doushantuo period, but the enhanced BSR would result in more extensive organic matter remineralization in the deep ocean of Nanhua Basin. This means that BSR facilitated the conversion of more organic matter with ^{13}C-depleted carbon to dissolved inorganic carbon (DIC) in the ocean, which was subsequently deposited as carbonate. There is no direct correlation between the Fe_{Py}/Fe_{HR} increasing and negative $\delta^{13}C_{carb}$ (carbon isotopic composition in carbonate) excursion in this study due to the lack of carbonate records, but previous studies revealed globally negative $\delta^{13}C_{carb}$ anomalies from the middle Ediacaran period (Grotzinger et al., 2011; Halverson et al., 2005; Johnston et al., 2012; Kaufman et al., 2007; Le Guerroué, 2010; Macdonald et al., 2010). In Nanhua basin, specifically, a Doushantuo negative carbon isotope excursion (DOUNCE) was widespread in various depositional settings ranging from coastal shallow basin, offshore intra-shelf basin to deepwater slope, characterized by a large shift in $\delta^{13}C_{carb}$ (from +5‰ down to −12‰) from the middle part of Doushantuo Formation (Jiang et al., 2007; Lu et al., 2013; McFadden et al., 2008; Zhou and Xiao, 2007; Zhu et al., 2007). If the Fe_{Py}/Fe_{HR} increase in the middle part of Doushantuo Formation can be correlated to DOUNCE, it is suggested that the negative $\delta^{13}C_{carb}$ excursion was caused by enhanced organic matter remineralization via BSR, which supports the previous hypothesis about the largest-known carbon isotope excursion in Earth's history (Fike et al., 2006; Jiang et al., 2007, 2008; McFadden et al., 2008).

5.2. The trace elements

Most redox sensitive elements in both sections have the concentrations close to or less than the average shale values, and thus their enrichment factors are equal to or less than 1 (Figs. 3 and 5). The lack of the enrichment of redox sensitive elements is generally considered as an indicator for the oxic depositional environment (Tribovillard et al., 2006). However, the oxic condition is incompatible with the moderate Mo enrichment and the iron speciation signatures in this study, and also inconsistent with the previous studies on the deep ocean in Nanhua basin (Han and Fan, 2015; Jiang et al., 2007, 2008; Li et al., 2010; McFadden et al., 2008). An alternative explanation is the "basin reservoir effect": in an isolated deep water, the sink flux of trace metals to the sediments generally exceeds the input associated with deep-water renewal, and thus the inventory of dissolved trace metals in the seawater could become depleted (Algeo and Lyons, 2006; Tribovillard et al., 2008). In this case, very few available trace elements are removed to the sediments in spite of anoxic conditions, and result in very low enrichment factors. However, it is not yet affirmative that the Nanhua basin is paleogeographically restricted based on current evidence. The persistent stratification and "sulfidic water wedge" at outer shelf/slope facies in the ocean may lead to an isolated deep ocean as well, obstructing the trace elements renewal in deep water (Li et al., 2010; Sahoo et al., 2016).

Mo and U are extensively used for paleoenvironmental reconstructions due to the well-established knowledge for their geochemical properties (Algeo and Maynard, 2004; Algeo and Tribovillard, 2009; Lyons et al., 2009; Partin et al., 2013; Piper and Calvert, 2009; Scott and Lyons, 2012; Tribovillard et al., 2012). The different uptake pathways of Mo and U from seawater cause their different magnitudes of enrichment in sediments or sedimentary rocks. Under conditions similar to the redox interface between Fe (III) and Fe (II), soluble U(VI) is reduced to insoluble U (IV) via microbial mediation, and then adsorption or precipitation as UO_2, U_3O_7, or U_3O_8 in sediment (Chaillou et al., 2002; Crusius et al., 1996; Klinkhammer and Palmer, 1991; McManus et al., 2005; Zheng et al., 2002). The removal Mo from seawater to the sediments prefers euxinic conditions, where the soluble MoO_4^{2-} are converted to particle-reactive thiomolybdates ($MoO_xS_{4-x}^{2-}$, x = 0–3) formation in the presence of free H_2S, and are then scavenged by sulfidized (S-rich) organic material or Fe–S phases (Erickson and Helz, 2000; Helz et al., 1996; Scott and Lyons, 2012; Tribovillard et al., 2004). Based on their characteristics in different modern marine systems, authigenic Mo-U (the uptake of Mo-U from seawater in the sediments) covariation patterns were developed to investigate the redox conditions and processes in ancient marine depositional systems (Algeo and Tribovillard, 2009; Han and Fan, 2015; Tribovillard et al., 2012). EF-Mo and EF-U are applied to describe the authigenic Mo-U, and three covariation patterns were identified in three typical modern marine settings (Algeo and Tribovillard, 2009; Tribovillard et al., 2012). For the "unrestricted marine" settings, authigenic U–Mo covariation is linked to the variation in benthic redox conditions: in suboxic conditions, EF-Mo and EF-U in sediments are low, and EF-Mo: EF-U ratios are less than that of seawater; in anoxic/euxinic conditions, the EF-Mo and EF-U in sediments increase, and EF-Mo: EF-U ratios are close to or exceed that of seawater (Fig. 10). For some weakly restricted basin, the EF-Mo: EF-U ratios in sediments are much higher than those of seawater due to a "particulate shuttle"

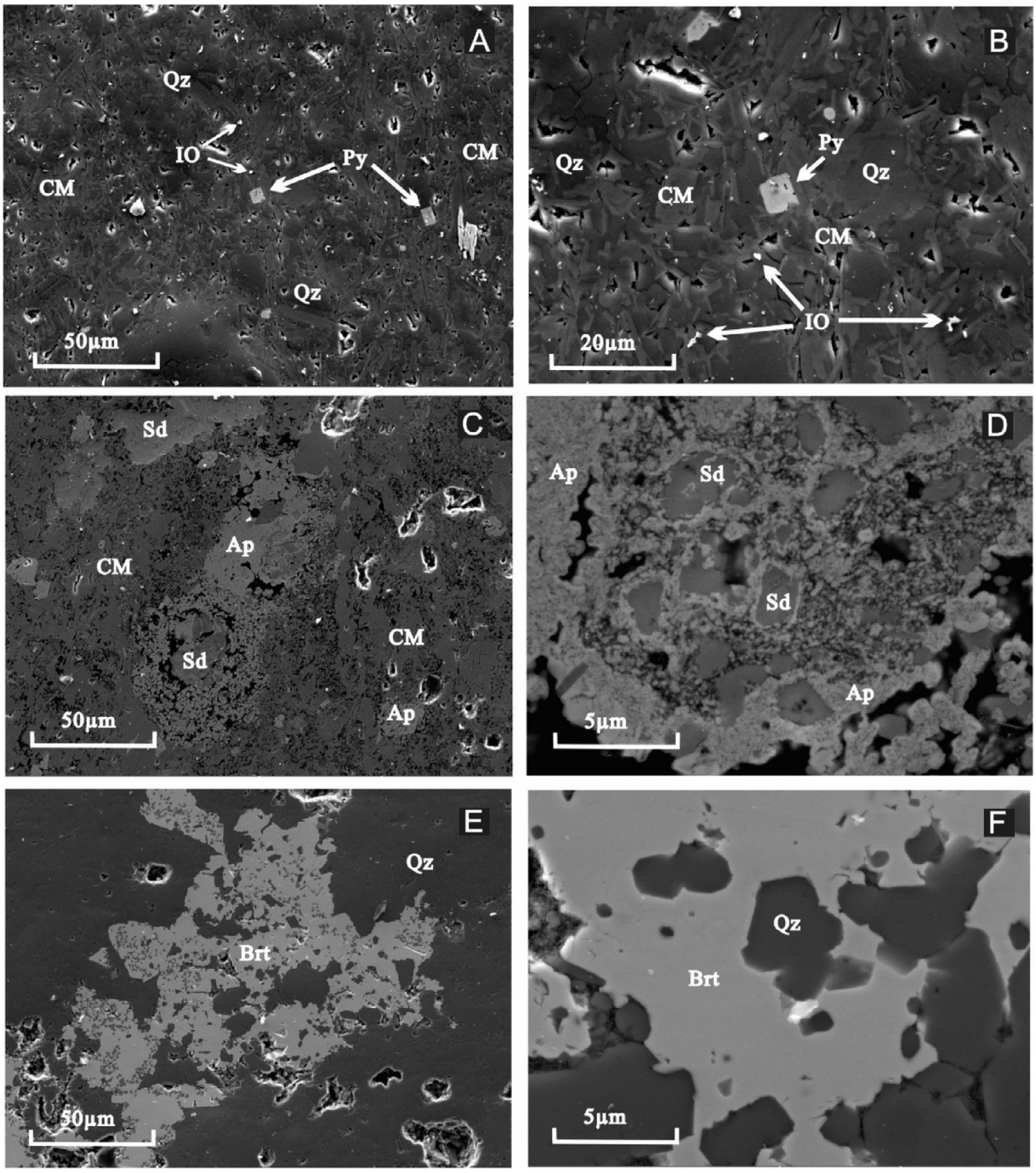

Fig. 7. The Scanning electron microscope (SEM) photos of the Longe shales. Py: Pyrite; IO: Iron Oxide; Qz: Quartz; CM: Clay Minerals; Brt: Barite; Sd: Siderite; Ap: Apatite.

(Fig. 10). For the strongly restricted basins, the EF-Mo: EF-U ratios are predominately controlled by the water mass chemistry.

The samples from the Longe and Jinjiadong sections show relatively high EF-Mo: EF-U ratios due to low EF-U (mostly <3) and moderate EF-Mo (~3–60), and their authigenic Mo-U patterns are similar to those from the modern Cariaco Basin and Orca Basin respectively (Fig. 10) (Algeo and Tribovillard, 2009; Tribovillard et al., 2012). The "basin reservoir effect" that we discussed above is also observed in the Cariaco Basin and Orca Basin (Algeo and Lyons, 2006; Little et al., 2015; Tribovillard et al., 2008), and has been used to explain the low U accumulation within the sediments (Algeo and Tribovillard, 2009; Tribovillard et al., 2012).

It also should be noted that our Fe speciation results and previous studies suggested a persistent anoxic deep water and relatively shallow chemocline depth (probably in the shelf margin-to-slope transition) in the Nanhua basin (Jiang et al., 2007, 2008; Li et al., 2010). In this large basin with a shallow chemocline, EF-Mo: EF-U ratios would mainly depend on the water chemistry (Algeo and Tribovillard, 2009). The modern Balck Sea and Cariaco Basin both have a shallow chemocline each in the water column. Below the chemocline, the Black Sea is strongly Mo-depleted in the seawater, but the Cariaco Basin has similar Mo concentration with its surface water (Algeo and Lyons, 2006; Little et al., 2015). The difference is possibly caused by two primary reasons: (1) the Cari-

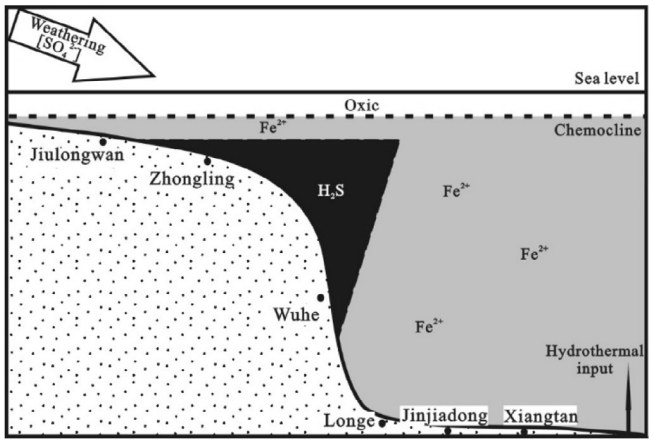

Fig. 8. Schematic representation for the "sulfidic water wedge" model of the Ediacaran Nanhua Basin.

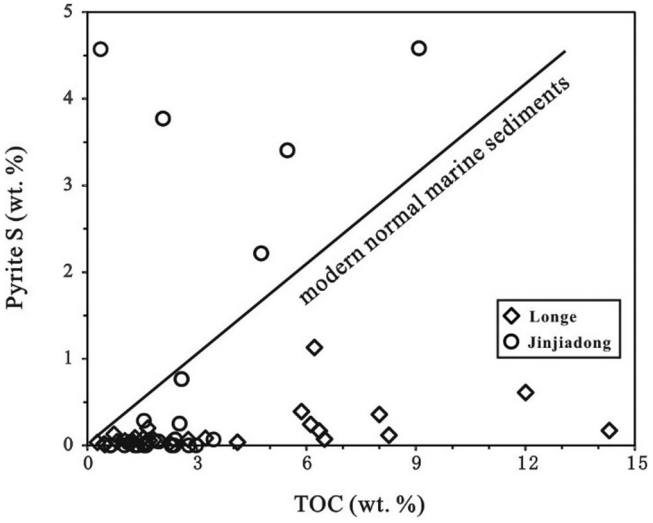

Fig. 9. Pyrite S contents versus TOC for samples from the Doushantuo black shales in the Longe and Jinjiadong sections.

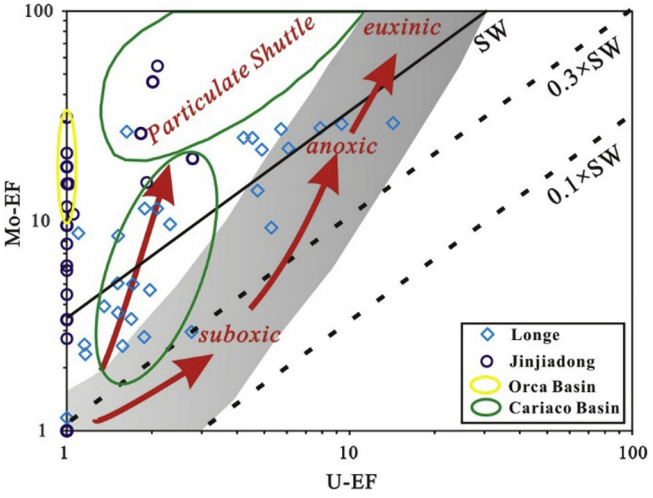

Fig. 10. EF-Mo versus EF-U for the Doushantuo black shales in the Longe and Jinjiadong sections, the average Mo/U weight ratio of seawater (SW) is 3.1 (Algeo and Tribovillard, 2009; Tribovillard et al., 2012).

aco Basin have much less H_2S concentrations than the Black Sea in the anoxic seawater, implying less Mo scavenging from seawater; (2) a fluctuated chemocline in the Cariaco Basin makes the "particulate shuttle" transporting Mo from shallow water to deep water through adsorption-desorption on the particulate Mn–Fe-oxyhydroxides form (Ho et al., 2004; Van Cappellen et al., 1998). Most samples in the Longe and Jinjiadong section have moderately enriched Mo concentrations (2–25 ppm), further supporting the non-euxinic depositional condition in deep Nanhua basin (Scott and Lyons, 2012). Comparing with the Black Sea, the Nanhua basin with ferruginous deep water is more analogous to a "weaker euxinic" Cariaco Basin, which is conducive to moderate Mo enrichment in seawater and related sediments.

6. Conclusion

We report new results for Fe speciation and trace element of the Doushantuo black shales from the Longe and Jinjiadong sections which were deposited in basin environments. Most samples in both sections show high Fe_{HR}/Fe_T ratios (>0.38), low Fe_{Py}/Fe_{HR} ratios (<0.7) and moderately enriched Mo concentrations (2–25 ppm), suggesting a predominately anoxic and ferruginous condition in the deep water of Nanhua basin during the Doushantuo period. Some samples in the basal, middle and top parts of the Jinjiadong section show high Fe_{Py}/Fe_{HR} ratios close to or exceeding 0.7, indicating that the condition changed to euxinic occasionally in the basin facies during the initial, middle and terminal Doushantuo period.

Fe_{Py}/Fe_{HR} ratios show an obvious increase in the middle part both in the Longe and Jinjiadong sections, indicating that the production of H_2S via bacteria sulfate reduction (BSR) in deep anoxic water was enhanced. If the Fe_{Py}/Fe_{HR} increasing can be correlated to DOUNCE in Nanhua basin, it is proved that the negative $\delta^{13}C_{carb}$ excursions from the middle of Ediacaran was caused by enhanced organic matter remineralization via BSR.

The different patterns of trace elements in the sediments may depend on contemporaneous water chemistry, which show similar to the modern Cariaco Basin. Most redox sensitive elements in the sediments of both sections have the enrichment factors are equal to or less than 1 because of their low concentrations, which may be caused by the obstructed renewal of trace elements in the isolated deep water. However, a "particulate shuttle" could overcome the "basin reservoir effect" limit through adsorption-desorption on the Mn–Fe-oxyhydroxides, sustaining the moderate Mo concentrations in the ferruginous deep ocean.

Acknowledgments

This research is supported by the National Basic Research Program of China (2013CB835003), the Natural Science Foundation of China (41373077, 41330102, 40532012, 41673002), the 111 project and the Fundamental Research Funds for the Central Universities. We thank for Prof. Zhang Qirui's help in field. We also appreciate the constructive suggestions from two anonymous reviewers.

References

Ader, M., Sansjofre, P., Halverson, G.P., Busigny, V., Trindade, R.I.F., Kunzmann, M., Nogueira, A.C.R., 2014. Ocean redox structure across the Late Neoproterozoic Oxygenation Event: a nitrogen isotope perspective. Earth Planet. Sci. Lett. 396, 1–13.

Algeo, T.J., Lyons, T.W., 2006. Mo–total organic carbon covariation in modern anoxic marine environments: implications for analysis of paleoredox and paleohydrographic conditions. Paleoceanography 21, 1–23. PA1016.

Algeo, T.J., Maynard, J.B., 2004. Trace-element behavior and redox facies in core shales of Upper Pennsylvanian Kansas-type cyclothems. Chem. Geol. 206, 289–318.

Algeo, T.J., Tribovillard, N., 2009. Environmental analysis of paleoceanographic systems based on molybdenum–uranium covariation. Chem. Geol. 268, 211–225.
Anderson, T.F., Raiswell, R., 2004. Sources and mechanisms for the enrichment of highly reactive iron in euxinic Black Sea sediments. Am. J. Sci. 304, 203–233.
Arnold, G.L., Brunner, B., Müller, I.A., Røy, H., 2014. Modern applications for a total sulfur reduction distillation method – what's old is new again. Geochem. Trans. 15, 1–12.
Berner, R.A., Raiswell, R., 1984. C/S method for distinguishing freshwater from marine sedimentary rocks. Geology 12, 365–368.
Canfield, D.E., 1998. A new model for Proterozoic ocean chemistry. Nature 396, 450–453.
Canfield, D.E., Berner, R.A., 1987. Dissolution and pyritization of magnetite in anoxic marine sediments. Geochim. Cosmochim. Acta 51, 645–659.
Canfield, D.E., Poulton, S.W., Narbonne, G.M., 2007. Late-neoproterozoic deep-ocean oxygenation and the rise of animal life. Science 315, 92–95.
Canfield, D.E., Poulton, S.W., Knoll, A.H., Narbonne, G.M., Ross, G., Goldberg, T., Strauss, H., 2008. Ferruginous conditions dominated later neoproterozoic deep-water chemistry. Science 321, 949–952.
Chaillou, G., Anschutz, P., Lavaux, G., Schäfer, J., Blanc, G., 2002. The distribution of Mo, U, and Cd in relation to major redox species in muddy sediments of the Bay of Biscay. Mar. Chem. 80, 41–59.
Chang, H.J., Chu, X.L., Feng, L.J., Huang, J., 2010. Iron speciation in cherts from the Laobao Formation, South China: implications for anoxic and ferruginous deep-water conditions. Chin. Sci. Bull. 55 (27–28), 3189–3196.
Chang, H.J., Chu, X.L., Feng, L.J., Huang, J., 2012. Progressive oxidation of anoxic and ferruginous deep-water during deposition of the terminal Ediacaran Laobao Formation in South China. Palaeogeogr. Palaeoclimatol. Palaeoecol. 321–322, 80–87.
Condon, D., Zhu, M.Y., Bowring, S., Wang, W., Yang, A.H., Jin, Y.G., 2005. U-Pb ages from the neoproterozoic Doushantuo Formation, China. Science 308, 95–98.
Crusius, J., Calvert, S., Pedersen, T., Sage, D., 1996. Rhenium and molybdenum enrichments in sediments as indicators of oxic, suboxic and sulfidic conditions of deposition. Earth Planet. Sci. Lett. 145, 65–78.
Erickson, B.E., Helz, G.R., 2000. Molybdenum(VI) speciation in sulfidic waters: stability and lability of thiomolybdates. Geochim. Cosmochim. Acta 64, 1149–1158.
Fan, H., Zhu, X., Wen, H., Yan, B., Li, J., Feng, L., 2014. Oxygenation of Ediacaran Ocean recorded by iron isotopes. Geochim. Cosmochim. Acta 140, 80–94.
Fike, D.A., Grotzinger, J.P., Pratt, L.M., Summons, R.E., 2006. Oxidation of the Ediacaran Ocean. Nature 444, 744–747.
Grotzinger, J.P., Fike, D.A., Fischer, W.W., 2011. Enigmatic origin of the largest-known carbon isotope excursion in Earth's history. Nat. Geosci. 4, 285–292.
Habicht, K.S., Canfield, D.E., 2001. Isotope fractionation by sulfate-reducing natural populations and the isotopic composition of sulfide in marine sediments. Geology 29, 555–558.
Habicht, K.S., Gade, M., Thamdrup, B., Berg, P., Canfield, D.E., 2002. Calibration of sulfate levels in the Archean Ocean. Science 298, 2372–2374.
Halverson, G.P., Hoffman, P.F., Schrag, D.P., Maloof, A.C., Rice, A.H.N., 2005. Toward a Neoproterozoic composite carbon-isotope record. Geol. Soc. Am. Bull. 117, 1181–1207.
Han, T., Fan, H., 2015. Dynamic evolution of the Ediacaran ocean across the Doushantuo Formation, South China. Chem. Geol. 417, 261–272.
Helz, G.R., Miller, C.V., Charnock, J.M., Mosselmans, J.F.W., Pattrick, R.A.D., Garner, C. D., Vaughan, D.J., 1996. Mechanism of molybdenum removal from the sea and its concentration in black shales: EXAFS evidence. Geochim. Cosmochim. Acta 60, 3631–3642.
Ho, T.-Y., Taylor, G.T., Astor, Y., Varela, R., Müller-Karger, F., Scranton, M.I., 2004. Vertical and temporal variability of redox zonation in the water column of the Cariaco Basin: implications for organic carbon oxidation pathways. Mar. Chem. 86, 89–104.
Huang, J., Chu, X., Lyons, T.W., Sun, T., Feng, L., Zhang, Q., Chang, H., 2013. The sulfur isotope signatures of Marinoan deglaciation captured in Neoproterozoic shallow-to-deep cap carbonate from South China. Precambr. Res. 238, 42–51.
Jiang, G., Sohl, L.E., Christie-Blick, N., 2003. Neoproterozoic stratigraphic comparison of the Lesser Himalaya (India) and Yangtze block (south China): Paleogeographic implications. Geology 31, 917–920.
Jiang, G.Q., Kaufman, A.J., Christie-Blick, N., Zhang, S.H., Wu, H.C., 2007. Carbon isotope variability across the Ediacaran Yangtze platform in South China: implications for a large surface-to-deep ocean delta C-13 gradient. Earth Planet. Sci. Lett. 261, 303–320.
Jiang, G.Q., Zhang, S.H., Shi, X.Y., Wang, X.Q., 2008. Chemocline instability and isotope variations of the Ediacaran Doushantuo basin in South China. Sci. China Ser. D 51, 1560–1569.
Jiang, G.Q., Wang, X.Q., Shi, X.Y., Zhan, S.H., Xiao, S.H., Dong, J., 2010. Organic carbon isotope constraints on the dissolved organic carbon (DOC) reservoir at the Cryogenian-Ediacaran transition. Earth Planet. Sci. Lett. 299, 159–168.
Jiang, G., Shi, X., Zhang, S., Wang, Y., Xiao, S., 2011. Stratigraphy and paleogeography of the Ediacaran Doushantuo Formation (ca. 635–551 Ma) in South China. Gondwana Res. 19, 831–849.
Johnston, D.T., Macdonald, F.A., Gill, B.C., Hoffman, P.F., Schrag, D.P., 2012. Uncovering the Neoproterozoic carbon cycle. Nature 483, 320–323.
Kaufman, A.J., Corsetti, F.A., Varni, M.A., 2007. The effect of rising atmospheric oxygen on carbon and sulfur isotope anomalies in the Neoproterozoic Johnnie Formation, Death Valley, USA. Chem. Geol. 237, 47–63.
Klinkhammer, G.P., Palmer, M.R., 1991. Uranium in the oceans: where it goes and why. Geochim. Cosmochim. Acta 55, 1799–1806.
Knoll, A.H., 1992. Biological and biogeochemical preludes to the Ediacaran radiation. In: Lipps, J.H., Signor, P.W. (Eds.), Origin and Early Evolution of the Metazoa. Springer, US, Boston, MA, pp. 53–84.
Le Guerroué, E., 2010. Duration and synchroneity of the largest negative carbon isotope excursion on Earth: The Shuram/Wonoka anomaly. C.R. Geosci. 342, 204–214.
Li, C., Love, G.D., Lyons, T.W., Fike, D.A., Sessions, A.L., Chu, X., 2010. A stratified redox model for the Ediacaran Ocean. Science 328, 80–83.
Little, S.H., Vance, D., Lyons, T.W., McManus, J., 2015. Controls on trace metal authigenic enrichment in reducing sediments: insights from modern oxygen-deficient settings. Am. J. Sci. 315, 77–119.
Lu, M., Zhu, M., Zhang, J., Shields-Zhou, G., Li, G., Zhao, F., Zhao, X., Zhao, M., 2013. The DOUNCE event at the top of the Ediacaran Doushantuo Formation, South China: broad stratigraphic occurrence and non-diagenetic origin. Precambr. Res. 225, 86–109.
Lyons, T.W., Anbar, A.D., Severmann, S., Scott, C., Gill, B.C., 2009. Tracking euxinia in the ancient ocean: a multiproxy perspective and Proterozoic case study. Annu. Rev. Earth Planet. Sci. 37, 507–534.
Macdonald, F.A., Schmitz, M.D., Crowley, J.L., Roots, C.F., Jones, D.S., Maloof, A.C., Strauss, J.V., Cohen, P.A., Johnston, D.T., Schrag, D.P., 2010. Calibrating the Cryogenian. Science 327, 1241–1243.
März, C., Poulton, S.W., Beckmann, B., Küster, K., Wagner, T., Kasten, S., 2008. Redox sensitivity of P cycling during marine black shale formation: dynamics of sulfidic and anoxic, non-sulfidic bottom waters. Geochim. Cosmochim. Acta 72, 3703–3717.
McFadden, K.A., Huang, J., Chu, X., Jiang, G., Kaufman, A.J., Zhou, C., Yuan, X., Xiao, S., 2008. Pulsed oxidation and biological evolution in the Ediacaran Doushantuo Formation. Proc. Natl. Acad. Sci. U.S.A. 105, 3197–3202.
McManus, J., Berelson, W.M., Klinkhammer, G.P., Hammond, D.E., Holm, C., 2005. Authigenic uranium: relationship to oxygen penetration depth and organic carbon rain. Geochim. Cosmochim. Acta 69, 95–108.
Och, L.M., Shields-Zhou, G.A., 2012. The Neoproterozoic oxygenation event: Environmental perturbations and biogeochemical cycling. Earth Sci. Rev. 110, 26–57.
Partin, C.A., Bekker, A., Planavsky, N.J., Scott, C.T., Gill, B.C., Li, C., Podkovyrov, V., Maslov, A., Konhauser, K.O., Lalonde, S.V., Love, G.D., Poulton, S.W., Lyons, T.W., 2013. Large-scale fluctuations in Precambrian atmospheric and oceanic oxygen levels from the record of U in shales. Earth Planet. Sci. Lett. 369–370, 284–293.
Piper, D.Z., Calvert, S.E., 2009. A marine biogeochemical perspective on black shale deposition. Earth Sci. Rev. 95, 63–96.
Poulton, S.W., Canfield, D.E., 2005. Development of a sequential extraction procedure for iron: implications for iron partitioning in continentally derived particulates. Chem. Geol. 214, 209–221.
Poulton, S.W., Canfield, D.E., 2011. Ferruginous conditions: a dominant feature of the ocean through Earth's history. Elements 7, 107–112.
Poulton, S.W., Raiswell, R., 2002. The low-temperature geochemical cycle of iron: from continental fluxes to marine sediment deposition. Am. J. Sci. 302, 774–805.
Qi, L., Hu, J., Gregoire, D.C., 2000. Determination of trace elements in granites by inductively coupled plasma mass spectrometry. Talanta 51, 507–513.
Raiswell, R., Canfield, D.E., 1998. Sources of iron for pyrite formation in marine sediments. Am. J. Sci. 298, 219–245.
Raiswell, R., Newton, R., Wignall, P.B., 2001. An indicator of water-column anoxia: Resolution of biofacies variations in the kimmeridge clay (Upper Jurassic, U.K.). J. Sediment. Res. 71, 286–294.
Raiswell, R., Newton, R., Bottrell, S.H., Coburn, P.M., Briggs, D.E.G., Bond, D.P.G., Poulton, S.W., 2008. Turbidite depositional influences on the diagenesis of Beecher's Trilobite Bed and the Hunsrück Slate; sites of soft tissue pyritization. Am. J. Sci. 308, 105–129.
Ries, J.B., Fike, D.A., Pratt, L.M., Lyons, T.W., Grotzinger, J.P., 2009. Superheavy pyrite ($\delta^{34}S_{pyr} > \delta^{34}S_{CAS}$) in the terminal Proterozoic Nama Group, southern Namibia: a consequence of low seawater sulfate at the dawn of animal life. Geology 37, 743–746.
Rothman, D.H., Hayes, J.M., Summons, R.E., 2003. Dynamics of the Neoproterozoic carbon cycle. Proc. Natl. Acad. Sci. U.S.A. 100, 8124–8129.
Sahoo, S.K., Planavsky, N.J., Kendall, B., Wang, X., Shi, X., Scott, C., Anbar, A.D., Lyons, T.W., Jiang, G., 2012. Ocean oxygenation in the wake of the Marinoan glaciation. Nature 489, 546–549.
Sahoo, S.K., Planavsky, N.J., Jiang, G., Kendall, B., Owens, J.D., Wang, X., Shi, X., Anbar, A.D., Lyons, T.W., 2016. Oceanic oxygenation events in the anoxic Ediacaran ocean. Geobiology. http://dx.doi.org/10.1111/gbi.12182.
Scott, C., Lyons, T.W., 2012. Contrasting molybdenum cycling and isotopic properties in euxinic versus non-euxinic sediments and sedimentary rocks: refining the paleoproxies. Chem. Geol. 324–325, 19–27.
Scott, C., Lyons, T.W., Bekker, A., Shen, Y., Poulton, S.W., Chu, X., Anbar, A.D., 2008. Tracing the stepwise oxygenation of the Proterozoic ocean. Nature 452, 456–459.
Shen, Y., Zhang, T., Hoffman, P.F., 2008. On the coevolution of Ediacaran oceans and animals. Proc. Natl. Acad. Sci. U.S.A. 105, 7376–7381.
Taylor, S.R., McLennan, S.M., 1985. The Continental Crust: Its Composition and Evolution. Blackwell Scientifc Publications.
Tribovillard, N., Riboulleau, A., Lyons, T., Baudin, F., 2004. Enhanced trapping of molybdenum by sulfurized marine organic matter of marine origin in Mesozoic limestones and shales. Chem. Geol. 213, 385–401.

Tribovillard, N., Algeo, T.J., Lyons, T., Riboulleau, A., 2006. Trace metals as paleoredox and paleoproductivity proxies: an update. Chem. Geol. 232, 12–32.
Tribovillard, N., Bout-Roumazeilles, V., Algeo, T., Lyons, T.W., Sionneau, T., Montero-Serrano, J.C., Riboulleau, A., Baudin, F., 2008. Paleodepositional conditions in the Orca Basin as inferred from organic matter and trace metal contents. Mar. Geol. 254, 62–72.
Tribovillard, N., Algeo, T.J., Baudin, F., Riboulleau, A., 2012. Analysis of marine environmental conditions based on molybdenum–uranium covariation—applications to Mesozoic paleoceanography. Chem. Geol. 324–325, 46–58.
Van Cappellen, P., Viollier, E., Roychoudhury, A., Clark, L., Ingall, E., Lowe, K., Dichristina, T., 1998. Biogeochemical cycles of manganese and iron at the oxic−anoxic transition of a stratified marine basin (Orca Basin, Gulf of Mexico). Environ. Sci. Technol. 32, 2931–2939.
Wang, J., Li, Z.-X., 2003. History of Neoproterozoic rift basins in South China: implications for Rodinia break-up. Precambr. Res. 122, 141–158.
Wignall, P.B., Newton, R., 1998. Pyrite framboid diameter as a measure of oxygen deficiency in ancient mudrocks. Am. J. Sci. 298 (7), 537–552.
Wilkin, R.T., Barnes, H.L., Brantley, S.L., 1996. The size distribution of framboidal pyrite in modern sediments: an indicator of redox conditions. Geochim. Cosmochim. Acta 60 (20), 3897–3912.
Wilkin, R.T., Arthur, M.A., Dean, W.E., 1997. History of water-column anoxia in the Black Sea indicated by pyrite framboid size distributions. Earth Planet. Sci. Lett. 148 (3–4), 517–525.
Xu, J., Zhu, S.-Y., Luo, T.-Y., Zhou, W., Li, Y.-L., 2015. Uranium mineralization and its radioactive decay-induced carbonization in a black shale-hosted polymetallic sulfide ore layer, Southwest China. Econ. Geol. 110, 1643–1652.
Zheng, Y., Anderson, R.F., van Geen, A., Fleisher, M.Q., 2002. Preservation of particulate non-lithogenic uranium in marine sediments. Geochim. Cosmochim. Acta 66, 3085–3092.
Zhou, C.M., Xiao, S.H., 2007. Ediacaran $\delta^{13}C$ chemostratigraphy of South China. Chem. Geol. 237, 89–108.
Zhu, M., Strauss, H., Shields, G.A., 2007. From snowball earth to the Cambrian bioradiation: calibration of Ediacaran-Cambrian earth history in South China. Palaeogeogr. Palaeoclimatol. Palaeoecol. 254, 1–6.